

Resonant Drift-Wave Coupling Modified by Nonlinear Separatrix Dissipation

A. A. Kabantsev,¹ T. M. O'Neil,¹ Yu. A. Tsidulko,² and C. F. Driscoll¹

¹Department of Physics, University of California at San Diego, La Jolla, California 92093, USA

²Budker Institute of Nuclear Physics, Novosibirsk, Russia

(Received 25 February 2008; published 5 August 2008)

Resonant drift-wave coupling experiments characterize a new dissipative coupling term caused by a trapping separatrix. The system is a cylindrical pure-electron plasma with an axial trapping separatrix generated by an applied θ -symmetric wall voltage. The resonant decay of $m_\theta = 2$ diocotron modes into $m_\theta = 1$ trapped-particle diocotron modes is measured and compared to parametric mode coupling theory. Experiments quantify the traditional nonlinear mode coupling term, plus a new separatrix-generated dissipative coupling term which is not yet characterized theoretically.

DOI: 10.1103/PhysRevLett.101.065002

PACS numbers: 52.35.Mw, 52.20.-j, 52.27.Jt, 52.55.Jd

Plasmas are inherently nonlinear, through the convective terms in the continuity or Vlasov equations. This non-dissipative nonlinearity gives rise to a plethora of mode couplings and instabilities which have been broadly studied. Specifically, the 3-wave parametric instability, which shows late-time energy sloshing and mode recurrences, has been analyzed theoretically [1,2], but less so experimentally.

Plasmas also generally contain magnetic and electric trapping separatrices, due to variations in magnetic field strength or external potentials. In toroidal fusion plasmas, the enhanced inboard magnetic field strongly constrains the poloidal rotation and gives rise to a variety of trapped-particle modes and induced currents. An early boundary-layer analysis of a trapping separatrix predicted near-discontinuous distribution functions, with damping effects scaling with collisionality and mode frequency as $(\nu/\omega)^{1/2}$ [3]. Later experimental work verified some aspects of trapped-particle modes (but not the damping) [4,5], and other scalings are predicted in other regimes [6].

Recent experiments on cylindrical pure-electron plasmas have characterized wave and transport effects from dissipation at controlled trapping separatrices, arising from either magnetic mirrors with $10^{-3} < \delta B_z/B_z < 10^{-1}$ or electrostatic barriers with $10^{-3} < \delta V_{\text{wall}}/\phi_0 < 1$. The separatrix dissipation enables and damps the trapped-particle diocotron mode (TPDM) [7,8] and damps $m \neq 0$ $k \neq 0$ plasma modes [9]. When combined with external θ asymmetries, the separatrix dissipation damps diocotron modes [10] and causes enhanced bulk plasma expansion and loss [11,12]. The boundary-layer analysis of TPDM damping agrees semiquantitatively with experiments [7,8], but experiments have not yet measured the separatrix distribution function discontinuity or unambiguously confirmed the $\nu^{1/2}$ scaling. Moreover, preliminary theory scalings for asymmetry-induced transport disagree with experiments, suggesting missing dissipative effects.

Here, we characterize these separatrix effects in a simple resonant mode coupling experiment. Specifically, we ob-

serve the resonant interaction between the traditional $k = 0$, $m = 2$ diocotron mode and the standing ($\pm k$) $m = 1$ TPDM, with a strong applied electrostatic trapping barrier. The initial parametric decay of the $m = 2$ pump wave into the two $m = 1$ daughter waves is adequately predicted by a conservative nonlinear coupling term V . However, fitting the late-time evolution requires (and quantifies) a *dissipative* nonlinear term K which is not yet characterized theoretically. This is likely the same as the dissipative coupling causing the *nonresonant* wave and transport effects referenced above, but no connecting theory is available.

The pure electron plasma columns described here are confined in a cylindrical Penning-Malmberg trap, as shown in Fig. 1. Electrons emitted from a hot tungsten source are confined radially by a nearly uniform axial magnetic field $2 \leq B \leq 18$ kG, and confined axially by negative voltages $V_c = -100$ V on end cylinders with wall radius $R_w = 3.5$ cm. Typical electron columns have length $L_p = 49$ cm and density $n_0 \approx 1.4 \times 10^7$ cm⁻³ over a radius $R_p = 1.2$ cm, giving line density $N_L \equiv \pi R_p^2 n_0 = 6 \times 10^7$ cm⁻¹.

The unneutralized electron charge results in a central potential $\phi_0 \approx -30$ V and in an $\mathbf{E} \times \mathbf{B}$ rotation of the

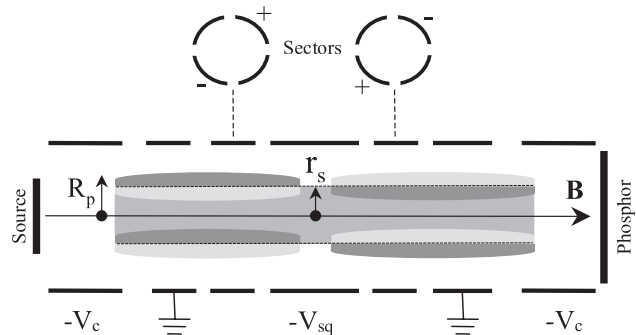


FIG. 1. Schematic of the cylindrical trap and electron plasma, with voltage $-V_{sq}$ creating an electrostatic separatrix. The TPDM is shown, with positive and negative trapped and untrapped density perturbations.

column at frequency $f_E(r) \leq f_{E0} \equiv cen_0/B = (36 \text{ kHz})(B/6 \text{ kG})^{-1}$. The electrons initially have a near-thermal velocity distribution, with $T \sim 0.5 \text{ eV}$, giving axial bounce frequency $f_b \equiv \bar{v}/2L_p \sim 300/\text{ms}$; but non-Maxwellian effects may be significant, since the electron-electron collisionality is weak, with $\nu_{ee} \lesssim 0.5/\text{ms}$.

A strong electrostatic trapping barrier is created by a “squeeze” voltage $V_{\text{sq}} \sim \phi_0/2$ applied to the central cylinder. Approximately $\frac{1}{2}$ of the electrons are trapped in one end or the other, and $\frac{1}{2}$ transit the full length. This trapping may be characterized by an end velocity $v_s(r)$ below which a particle is trapped; or more coarsely by a radius R_s outside of which *all* particles are trapped. The trapping separatrix causes the nonlinear dissipative coupling term studied here, and enables the TPDM, which we utilize because of its adjustable frequency.

Waves are excited and detected using electrodes with 4 and 8 isolated θ sectors. The waves of interest are the traditional $m = 2, k = 0$ diocotron mode and the standing $m = 1$ TPDM. These are $\mathbf{E} \times \mathbf{B}$ drift modes, where the drifting (d) perturbed density $\delta n_m^{(d)}$ varies as

$$\delta n_m^{(d)}(r, \theta, z, t) = A_m^{(d)}(\tau) \partial n_0 / \partial r \cos\{m\theta - \omega_m t + \theta_m(\tau)\} Z(z), \quad (1)$$

where we denote the $(10 \times)$ slower variations by τ . The $m = 2$ mode at frequency f_2 is uniform over the entire plasma length, and so has $Z(z) = 1$. As shown in Fig. 1, the axially split (a) $m = 1$ TPDM at frequency f_{1a} exhibits 180° -shifted drift motion on either end of the trapping barrier, so $Z(z) = \text{sgn}(z - L_p/2)$; this represents two counter-propagating waves with wave numbers $\pm \pi/L_p$, plus harmonics. The TPDM is distinct from the traditional $m = 1, k = 0$ diocotron mode at frequency $f_d = (R_p/R_w)^2 f_E \sim 0.1 f_E$, which would have $Z(z) = 1$. Also, the TPDM is partially shielded by untrapped (u) particles at $r < R_s$, giving an additional kinetic component $\delta n_{1a}^{(u)}(r, \theta, z, t)$ to the eigenfunction, with $\delta n_{1a}^{(u)} \sim \mathcal{O}(\delta n_{1a}^{(d)})$. The TPDM frequency depends on the number of axially trapped particles, and can be tuned to obtain the desired resonance $f_{1a} = f_2/2$. Small changes in V_{sq} then provide adjustable resonance detuning, characterized by $\Delta f \equiv (f_2 - 2f_{1a})$.

We characterize the mode amplitudes by the displacements A_1 and A_2 of Eq. (1) which would give the received wall signal V_s . The received wall-sector waveform $V_s(t)$ will be directly fit by theory, but for presentation we display mode amplitudes and phases V_m and Θ_m , where $V_s(t) = \sum_m V_m(\tau) \cos\{2\pi f_m t + \Theta_m(\tau)\}$. For $m = 1$, Eq. (1) represents a rigid displacement of $n_0(r)$ by a distance A_1 ; this produces a wall electric field $E_{\text{rw}} = (4eN_L/R_w)(A_1/R_w)$ giving sector voltage $V_1 = c_1 A_1$ with $c_1 = 0.69 \text{ mV/mm}$ for our plasmas and receiver electronics. For $m = 2$, Eq. (1) represents an elliptical distortion, so a water-bag plasma would have (major, minor)

radii $(a, b) = R_p \pm A_2$, giving a field $E_{\text{rw}} = (4eN_L/R_w) \times (2A_2 R_p/R_w^2)$; for our $n_0(r)$ profiles, this gives $V_2 = c_2 A_2$ with $c_2 = 0.31 \text{ mV/mm}$.

A camera diagnostic verifies the calibration of these moments, and gives the wave density eigenfunctions. At time t_d , the electron column (or just the right half of it) is dumped onto a phosphor screen imaged with a CCD camera, giving the two-dimensional z -integrated density $\bar{n}(r, \theta, t_d)$. For the TPDM, the amplitude A_{1a} represents the *net* dipole moment from $\delta n_{1a}^{(d)} + \delta n_{1a}^{(u)}$, as measured by the camera and the wall sectors.

Figure 2 shows the parametric decay that results when an $m = 2$ pump wave is driven to amplitude $A_2 = 0.66 \text{ mm}$ by a 30-cycle burst at $f_2 = 42 \text{ kHz}$. The points are the mode amplitudes $A_{1a}(\tau)$ and $A_2(\tau)$ obtained from the wall-sector voltage $V_s(t)$. The TPDM daughter wave initially grows exponentially from noise, as $A_{1a} \propto \exp\{\Gamma_{1a} t\}$, with $\Gamma_{1a} = 4.8/\text{ms}$. When A_{1a} becomes comparable to A_2 , the energy coupling direction reverses, giving a complicated late-time evolution. Our major conclusion is that the late-time evolution differs significantly from the predictions of standard parametric mode coupling theory (dashed curves), and that an additional dissipative coupling term \mathbf{K} is required to fit the data (solid curves).

To see this, we first sketch the simplest nonlinear analysis, using a *nondissipative* “square density profile” model. The model assumes a cold drifting plasma with density $n(r) = n_0$ for $r \leq R_p$, and abrupt complete trapping for $r > R_s$. The waves then consist of perturbed surface charge density $\delta n_m^{(d)}$ at $r = R_p$ and $r = R_s$. For the TPDM mode, Debye shielding from untrapped par-

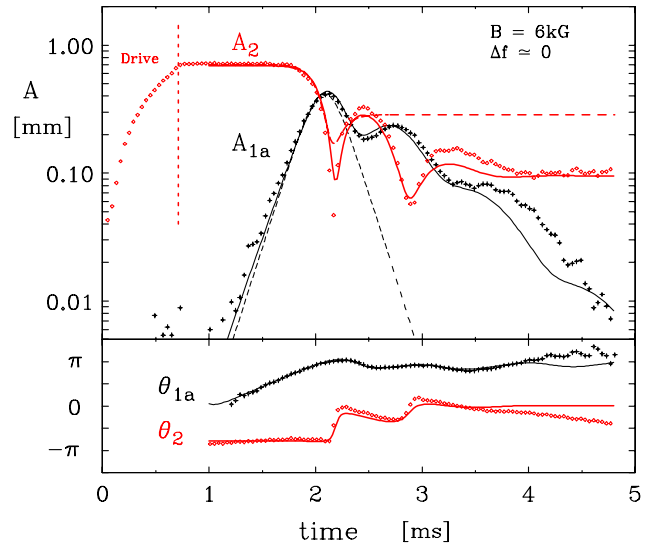


FIG. 2 (color online). Amplitudes and phases during parametric decay of $m = 2$ diocotron pump wave into $m = 1$ TPDM daughter wave. Points are measured data; solid curves are Eq. (3); dashed curves are Eq. (3) with $\mathbf{K} = 0$.

ticles gives $\delta\phi(r < R_s) = 0$, and an approximation of $\delta\phi(R_s) = 0$ replaces a calculation of $\delta n^{(u)}$ for $r < R_s$. Poisson's equation and the continuity equation, plus the boundary conditions at $r = 0$ (or $r = R_s$) and $r = R_w$, then determine simple expressions for the frequencies, mode eigenfunctions $\delta\phi_m(r, t)$, and mode couplings. The frequencies f_{1a} and f_2 are given by

$$\begin{aligned} f_{1a} &= f_E [1 - (\rho_p^2 - \rho_s^2)(1 - \rho_p^2)/(1 - \rho_s^2)\rho_p^2] \approx 0.5f_{E0}, \\ f_2 &= f_E [1 - \rho_p^4] \approx f_{E0}, \end{aligned} \quad (2)$$

where $\rho_p \equiv R_p/R_w = 0.34$ and $\rho_s \equiv R_s/R_w = 0.24$.

In this simple model, nonlinearity arises only from the continuity equation, and it causes mode couplings \mathbf{V} , as expected. However, the model ignores collisional interaction between trapped and untrapped particles, which is known to cause damping of the TPDM [8]; here, we simply add an *ad hoc* damping rate γ_{1a} . Measurements of TPDM decay with no other modes present give $\gamma_{1a}(B) = (-1.4/\text{ms})(B/6 \text{ kG})^{-1/2}$. Moreover, the model also ignores nonlinear coupling effects of the dissipative separatrix, as the modes themselves nonlinearly influence the separatrix scatterings.

Here, we posit the simple nonlinear dissipative terms \mathbf{K} shown in Eq. (3), motivated by experiments and constrained by analytic self-consistency. Square-profile theory with *ad hoc* damping γ_{1a} and *ad hoc* nonlinear dissipative couplings \mathbf{K} then gives the coupled amplitude equations

$$\begin{aligned} \frac{dA_{1a}}{dt} &= -\frac{\omega_{E0}}{R_w} (i\mathbf{V} + \mathbf{K}) A_{1a}^* A_2 e^{-i\Delta\omega t} + \gamma_{1a} A_{1a}, \\ \frac{dA_2}{dt} &= -\frac{\omega_{E0}}{R_w} (i\mathbf{V} + \mathbf{K}) A_{1a}^2 e^{+i\Delta\omega t}. \end{aligned} \quad (3)$$

Theory gives a rough estimate of $\mathbf{V} \approx \rho_p(1 + \rho_p^2) \sim 0.4$. In Eq. (3), the detuning $\Delta\omega$ is assumed to be small, as is $(dA/dt)/A$. The predicted initial growth rate Γ_{1a} is

$$\begin{aligned} (\Gamma_{1a} - \gamma_{1a})^2 &= \Gamma_0^2 - \pi^2 \Delta f^2, \\ \text{with } \Gamma_0 &\equiv \frac{\omega_{E0}}{R_w} (\mathbf{V}^2 + \mathbf{K}^2)^{1/2} |A_2|. \end{aligned} \quad (4)$$

Figure 3 shows the measured growth rates Γ_{1a} versus pump amplitude A_2 , for 3 magnetic fields, when tuned to resonance $\Delta f = 0$. We find $\Gamma_{1a} \propto A_2$ and $\Gamma_{1a} \propto B^{-1}$ with offsets γ_{1a} , as predicted by Eq. (4). Using the separately measured $\gamma_{1a}(B)$, the 3 dashed lines of Fig. 3 represent Eq. (4) with a single fit parameter $(\mathbf{V}^2 + \mathbf{K}^2)^{1/2} = 1.27$.

Figure 4 shows the dependence of this initial growth rate on resonance detuning Δf to be quantitatively consistent with parametric decay theory. Here, linear mode measurements give $\Delta f = (4.06 \text{ kHz}/V)(V_{\text{sq}} - 14.V)$, and the short-dashed lines are Eq. (4) with Γ_0 set by the $B = 2 \text{ kG}$ fit (short-dashed lines) of Fig. 3, i.e., $(\mathbf{V}^2 + \mathbf{K}^2)^{1/2} = 1.13$. The experimental \mathbf{V} 's are about $3\times$ larger than the simple model estimate, since \mathbf{K} will be seen to be small.

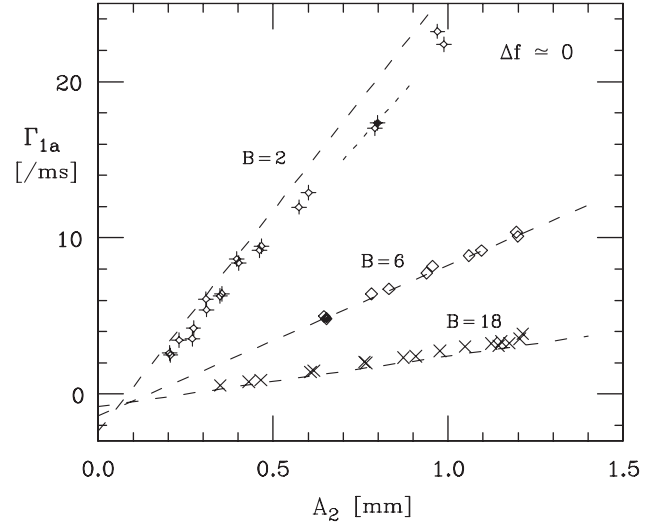


FIG. 3. Measured TPDM growth rate $\Gamma_{1a}(B)$ versus pump amplitude A_2 , for 3 magnetic fields. Dashed lines represent Eq. (4) with $(\mathbf{V}^2 + \mathbf{K}^2)^{1/2} = 1.27$ and the measured $\gamma_{1a}(B)$.

We now consider the late-time evolutions as in Fig. 2, to obtain the dissipative coupling term \mathbf{K} . We fit the received $V_s(t)$ to the waveform generated by Eq. (3) with fit parameters \mathbf{V} , \mathbf{K} , γ_{1a} , $A_{1a}(0)$, f_{1a} , $\theta_{1a}(0)$, $A_2(0)$, f_2 , $\theta_2(0)$, with $\Delta\omega \equiv 2\pi(f_2 - 2f_{1a})$ and $\omega_{E0} \equiv 2\pi f_2$. The waveforms span hundreds of wave cycles, so A , f , θ are unambiguous. For Fig. 2, optimization gives $\mathbf{V} = 1.6$, $\mathbf{K} = 0.44$, $\gamma_{1a} = -1.6/\text{ms}$, and $\Delta\omega = 2\pi \times 1 \text{ kHz}$, even though Δf was experimentally tuned to zero using separate linear modes. The solid lines show the mode amplitudes and phases for the optimal waveform; Eq. (3) fits the received waveform $V_s(t)$ accurately, maintaining phase coherence over ~ 100 cycles of f_2 .

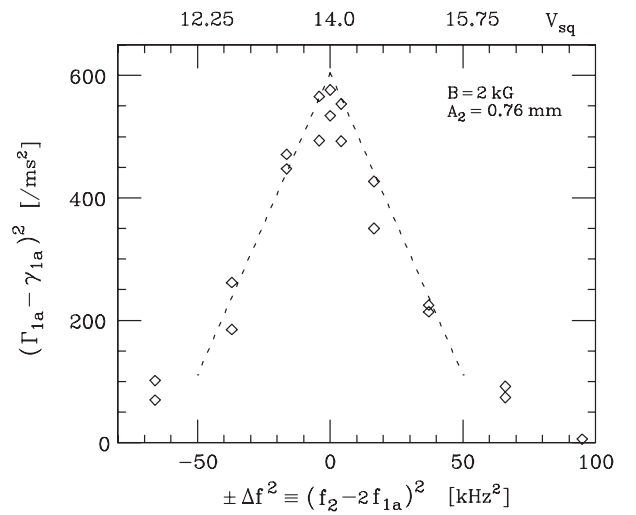


FIG. 4. Measured decrease in growth rate Γ_{1a} with resonance detuning Δf^2 (points) obtained by varying V_{sq} ; dashed line is Eq. (4) as in Fig. 3.

TABLE I. Parameters V , K , γ_{1a} of Eq. (3) obtained from near-resonant wave evolutions at $B = 2, 6, 18$ kG.

B [kG]	V	K	$-\gamma_{1a}$ [ms]
2	1.4 ± 0.1	0.29 ± 0.05	3.1 ± 0.4
6	1.7 ± 0.1	0.47 ± 0.1	1.7 ± 0.1
18	1.8 ± 0.2	0.47 ± 0.1	1.0 ± 0.1

The dashed lines of Fig. 2 show an analogous fit with $K = 0$ (fit over $1 < t < 2.4$ ms, then extended), giving $V = 1.88$ and $\gamma_{1a} = -2.9$ /ms. Here, the fit diverges from $V_s(t)$ on the first energy exchange, as the fit loses phase coherence with the $m = 2$ mode. Analysis of about 200 evolutions in various regimes demonstrates conclusively that a dissipative coupling term such as K is required to approximate the observed late-time evolutions.

The fits have average errors $\delta V_s(t)$ about 3%–10% of the average magnitude of $V_s(t)$. The resulting V and K parameters vary by $\pm 10\%$ for different fitting periods or for repeated experiments. We believe these variations arise more from missing nonlinear coupling terms than from experimental errors or irreproducibility. For any given evolution, a 20% change in K fully destroys the correspondence with the late-time energy sloshing, no matter how other parameters are varied. For technical reasons, several other fitting parameters representing voltage offsets, 60 Hz noise, and filtration phase shifts are sometimes used, but these are orthogonal to the evolution of Eq. (3).

Fits to near-resonant evolutions at $B = 2, 6,$ and 18 kG show that both V and K are approximately independent of B , as given in Table I. This constant V multiplying $\omega_{E0} \propto B^{-1}$ in Eq. (3) is expected for $\mathbf{E} \times \mathbf{B}$ drift processes. However, the K scaling has no theory basis as yet.

We have verified that K arises from the same ‘‘collisional’’ separatrix dissipation as γ_{1a} , by rf enhancement of separatrix crossings. Prior experiments [11] demonstrated that an external rf drive caused enhanced separatrix crossings around $v_s = f_{\text{rf}} L_p$, thereby increasing $|\gamma_{1a}|$ and proportionately increasing asymmetry-induced plasma expansion rates ν_p . Here, for $B = 2$ and 6 kG, we find that a moderate amplitude rf drive doubles γ_{1a} and increases K by about 75%. For $B = 18$ kG, the effects on γ_{1a} and K were masked by direct rf coupling to the modes.

Phase-locked energy sloshing between modes is a characteristic of nonlinear coupling equations. A theory fit with $\gamma_{1a} = K = 0$ in Fig. 2 would show recurrent growth and decay of A_{1a} and A_2 , with recurrence time determined by the slope Γ_{1a} and by the (unphysical) minimum value of A_{1a} . The energy loss apparent in Fig. 2 is largely due to γ_{1a} . Indeed, an energy accounting of $A_{1a}^2 + A_2^2 - 2 \int dt \gamma_{1a} A_{1a}^2$ is almost constant with time for Fig. 2 and

all other evolutions. This implies that the energy dissipation resulting from K is small, although the resulting phase shifts are crucial, determining the observed recurrence times. We note also that a ‘‘generic’’ term added to Eq. (3) would not conserve energy and would give wildly unstable time evolutions. Although *ad hoc* theoretically, the K terms mandated experimentally are from a highly constrained set of possibilities.

Finally, we reiterate that the K terms in Eq. (3) are probably just the first in a series of resonant and *nonresonant* dissipative couplings which contribute to parametric decay and to other damping and transport effects. For example, a nonresonant term $dA_{1a}/dt \propto K_{\text{NR}} |A_2| |A_{1a}|$ is anticipated, representing the A_2 dependence of γ_{1a} . The fitted γ_{1a} values of Table I are substantially larger than the γ_{1a} values obtained from single mode decays, because here the missing nonresonant terms ‘‘fit’’ best into γ_{1a} ; indeed preliminary experiments show increased TPDM damping rates $|\gamma_{1a}|$ when a (nonresonant) $m = 2$ mode is also launched. Similarly, the V term itself is larger from the late-time fits than from early growth rates, also suggesting missing terms. As theory and experiments progress, we anticipate a more unified perspective on the various trapped-particle-mediated damping and transport effects.

This work was supported by National Science Foundation Grant No. PHY0354979.

-
- [1] R. Z. Sagdeev and A. A. Galeev, *Nonlinear Plasma Theory* (W.A. Benjamin, New York, 1969), Chap. 1.
 - [2] R. N. Franklin, Rep. Prog. Phys. **40**, 1369 (1977).
 - [3] M. N. Rosenbluth, D. W. Ross, and D. P. Kostomarov, Nucl. Fusion **12**, 3 (1972).
 - [4] J. Slough, G. A. Navratil, and A. K. Sen, Phys. Rev. Lett. **47**, 1057 (1981).
 - [5] G. A. Navratil, A. K. Sen, and J. Slough, Phys. Fluids **26**, 1044 (1983).
 - [6] H. E. Mynick, Phys. Plasmas **13**, 058102 (2006).
 - [7] A. A. Kabantsev, C. F. Driscoll, T. J. Hilsabeck, T. M. O’Neil, and J. H. Yu, Phys. Rev. Lett. **87**, 225002 (2001).
 - [8] T. J. Hilsabeck, A. A. Kabantsev, C. F. Driscoll, and T. M. O’Neil, Phys. Rev. Lett. **90**, 245002 (2003).
 - [9] A. A. Kabantsev and C. F. Driscoll, Phys. Rev. Lett. **97**, 095001 (2006).
 - [10] A. A. Kabantsev and C. F. Driscoll, Trans. Fusion Sci. Technol. **47**, 263 (2005).
 - [11] A. A. Kabantsev and C. F. Driscoll, Phys. Rev. Lett. **89**, 245001 (2002).
 - [12] C. F. Driscoll, A. A. Kabantsev, T. J. Hilsabeck, and T. M. O’Neil, in *Non-Neutral Plasma Physics V*, edited by M. Schauer *et al.*, AIP Conf. Proc. No. 692 (AIP, New York, 2003) p. 3.